AGU ADVANCING EARTH AND SPACE SCIENCE

Water Resources Research

RESEARCH ARTICLE
10.1029/2020WR029430

Rationalizing the Differences Among Hydraulic Relationships Using a Process-Based Model

Fan Xu[1], Giovanni Coco[2], Ian Townend[1,3,4], Leicheng Guo[1], Qing He[1], Kun Zhao[4,5], and Zeng Zhou[4,5]

[1]State Key Laboratory of Estuarine and Coastal Research, East China Normal University, Shanghai, China, [2]Faculty of Science, University of Auckland, Auckland, New Zealand, [3]School of Ocean and Earth Sciences, University of Southampton, Southampton, UK, [4]State Key Laboratory of Hydrology-Water Resources and Hydraulic Engineering, Hohai University, Nanjing, China, [5]College of Harbor, Coastal and Offshore Engineering, University of Hohai, Nanjing, China

Key Points:

- Theoretical expressions of both at-a-station hydraulic geometry (AHG) and downstream hydraulic geometry (DHG) are derived
- The theoretical expressions of AHG provides a physical explanation for at-many-stations hydraulic geometry
- The different behaviors of AHG and DHG are attributed to the lateral adjustment of the bank and flow turbulence, respectively

Supporting Information:

Supporting Information may be found in the online version of this article.

Correspondence to:

F. Xu,
fan.xu@sklec.ecnu.edu.cn

Citation:

Xu, F., Coco, G., Townend, I., Guo, L., He, Q., Zhao, K., & Zhou, Z. (2021). Rationalizing the differences among hydraulic relationships using a process-based model. *Water Resources Research*, *57*, e2020WR029430. https://doi.org/10.1029/2020WR029430

Received 10 DEC 2020
Accepted 10 JUL 2021

Abstract The use of power law forms to describe hydraulic geometry is a classic subject with a history of over 70 years. Two distinct forms of power laws have been proposed: at-a-station hydraulic geometry (AHG) and downstream hydraulic geometry (DHG). Although the utility of these semiempirical expressions is widely recognized, they remain poorly understood in terms of the mechanisms underlying the differences between AHG and DHG, as well as the variability among different systems. In this study, we attempt to address these basic issues. Two hypotheses are proposed: (a) the different geomorphic relationships represented by AHG and DHG result from the control of lateral adjustment of the bank and flow turbulence over short and long timescales, respectively; and (b) the systematic variability of the AHG and DHG exponents is related to the description of the frictional resistance. These two hypotheses are embedded in our theoretical models and lead to explicit functional forms for AHG and DHG. The verification of our hypotheses is based on a large data set consisting of over 550 *b*-*f*-*m* exponents and 120 power law hydraulic relations. The analysis highlights the role of uncertainties in data acquisition and theoretical/statistical explanations. In addition, the theoretical expressions of AHG also provide an explanation of at-many-stations hydraulic geometry (AMHG) in a physical sense. Overall, our work provides new insights into the fundamental theory of power laws and hydraulic geometry.

1. Introduction

An ancient Chinese proverb states: "Don't push the river, it flows by itself." Scientists and engineers have long struggled to fully translate the second part of the proverb into a mathematical description. Leopold and Maddock (1953) linked the time-varying measurements of instantaneous river width B, depth H and velocity U at a gauging station to the corresponding discharge Q using simple power functions, and termed such empirical relationships as at-a-station hydraulic geometry (denoted as "AHG" hereafter). At the same time, the authors created downstream hydraulic geometry (denoted as "DHG" hereafter) to describe the hydraulic relations with bankfull (or mean annual) B, H, U, and Q downstream along a river. The fundamental difference between these two relationships is that AHG deals with temporal variability while DHG focuses on spatial variability. In addition, the mean annual or bankfull parameters used in DHG generally have a longer returning period than the time-varying parameters of AHG. Despite their conceptual difference, both AHG and DHG were expressed by the same well-known functional forms:

$$\begin{cases} B = aQ^b, \\ H = cQ^f, \\ U = kQ^m, \end{cases} \tag{1}$$

where the coefficients a, c, and k, and the exponents b, f, and m are fitting parameters. Given $Q = BHU$, it can be deduced that $ack = 1$ and $b + f + m = 1$. The AHG and DHG parameters will be distinguished by subscripts when necessary (i.e., b_s, f_s, and m_s for AHG and b_d, f_d, and m_d for DHG).

Many researchers have verified the goodness of fit of such empirical relationships based on the measurements from numerous rivers characterized by different physiographic settings (Ackers, 1964; Andreadis

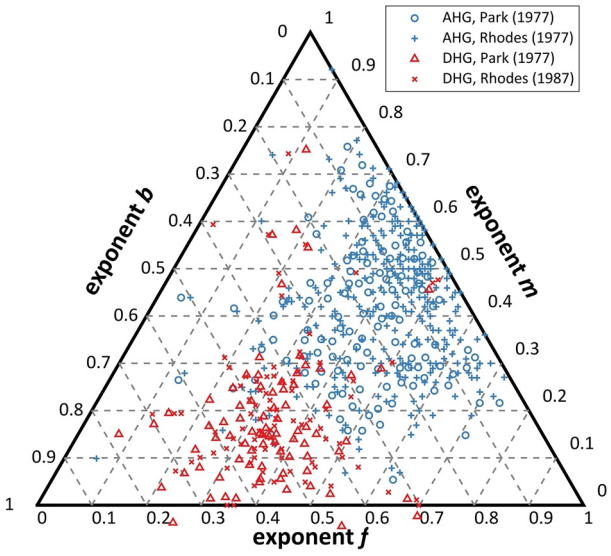

Figure 1. *b-f-m* ternary diagram of the at-a-station hydraulic geometry (blue dots) and downstream hydraulic geometry (red dots) exponents, redrawn from Park (1977) and Rhodes (1977, 1987).

et al., 2013; Clifford, 1996; Eaton, 2013; Fahnestock, 1963; Hey & Thorne, 1986; Kellerhals, 1967; Leopold & Miller, 1956; Sherwood & Huitger, 2005; Stevens, 1989; Williams, 1978; Wolman & Brush, 1961). Park (1977) and Rhodes (1977, 1987) collated existing observations to develop a *b-f-m* ternary diagram consisting of over 400 AHG exponents and 150 DHG exponents (Figure 1). The AHG and DHG exponents occupy different parts of the ternary diagram with limited overlap. This implies that AHG and DHG are intrinsically representative of different conditions.

Both the AHG and DHG *b-f-m* exponents exhibit highly scattered distributions in the ternary diagram (Figure 1) and no clear trend can be observed. Studies usually averaged the fitted *b-f-m* exponents from different systems (Ferguson, 1986; Leopold & Maddock, 1953), or introduced additional parameters (e.g., sediment grain size) attempting to construct unified power law relationships (Millar, 2005; Parker et al., 2007). Some additional insights were provided by Jung et al. (2013) and Kim and Paik (2018), who explored the variation in suspended sediment concentration for systems characterized by $b_d > f_d$ and $b_d < f_d$, respectively. Efforts have also been made to deduce the analytical solutions of *b-f-m* exponents through hydraulic equations (Gleason, 2015). Studies on AHG generally concentrate on the variability of the hydraulic variables with the short-term rise and fall of water level (Dingman, 2007; Ferguson, 1986). For example, Ferguson (1986) preset a parabolic channel cross section and deduced that $(b_s, f_s, m_s) = (0.23, 0.46, 0.31)$, with $b_s = f_s/2$. On the other hand, studies on DHG primarily emphasize the long-term morphodynamic equilibrium of the channel profiles and the associated bankfull geometry and kinematics (Cao & Knight, 1996; Finnegan et al., 2005; Huang et al., 2002; Langbein, 1963; Millar, 2005; Savenije, 2003).

In contrast to the extensive attention for *b-f-m* exponents, researchers have shown much less interests in the *a-c-k* coefficients of AHG or DHG (Equation 1). This might be attributed to the large variability in the fitted values of the *a-c-k* coefficients, ranging from 10^0 to 10^3 (Gleason & Smith, 2014; Rhoads, 1991; Stewardson, 2005). A notable progress was provided by Gleason and Smith (2014), who plotted a series of fitted AHG parameters along a river in a semilog coefficient-exponent diagram and observed that b_s, f_s, and m_s indicate strong linear decrease with $\log a_s$, $\log c_s$, and $\log k_s$, respectively. Gleason and Smith (2014) termed this finding as at-many-stations hydraulic geometry (denoted as "AMHG" hereafter) and further developed a statistical tool to evaluate the discharge based on channel width data, which can be derived from remote sensing images. Barber and Gleason (2018) confirmed that AMHG is a common phenomenon among 191 natural fluvial systems in the continental United States.

Much of our understanding of hydraulic geometry has so far stemmed from fitting power laws to field measurements. However, such data-driven analyses do not address fundamental questions like: "Why do power functions represent these geomorphic relationships?," "Do *b-f-m* exponents vary systematically between different systems?," "Why do AHG and DHG exponents exhibit different distributions in the *b-f-m* ternary diagram?" and "How are the *a-c-k* coefficients physically related to *b-f-m* exponents?" (Gleason & Smith, 2014; Park, 1977; Parker et al., 2007; Rhodes, 1977, 1987; Richards, 1973). Existing theoretical approaches often preassume the existence of power functions of the discharge (Cao & Knight, 1996; Ferguson, 1986; Finnegan et al., 2005; Huang et al., 2002; Langbein, 1963; Millar, 2005; Savenije, 2003) and/or constrain the channel cross section to be a particular shape, such as a rectangle (e.g., Cao & Knight, 1996; Huang et al., 2002; Langbein, 1963), trapezium (e.g., Eaton et al., 2004) or parabola (e.g., Dingman, 2007). Therefore, these are still room to develop a general analytical approach to address these underlying questions.

In this study, we attempt to gain some explanatory insights into the use of the power law in hydraulic geometry. Two hypotheses are proposed in terms of the hydrodynamic and sedimentary processes that may be responsible for the power law relationships exhibited by AHG and DHG (see Section 2 for a detailed description). The theoretical models are developed attempting to derive the functional forms of AHG and

DHG. Moreover, in addition to the data sets of *b-f-m* exponents shown in Figure 1, we collate up to 120 sets of complete power law relationships with both *b-f-m* exponents and *a-c-k* coefficients (see Tables 1 and 2). The derived functional forms are compared with the data sets, as a verification of these hypotheses and with the previous, related work by Jung et al. (2013). Our objective is to develop a more robust explanation that brings new insights into these geomorphic/hydraulic relationships.

2. Methods

2.1. Hypotheses

2.1.1. Hypothesis 1: Fast and Slow Processes

The evolution of a channel cross section depends on two key processes: (a) erosion/deposition of stream bed driven by the flow turbulence, and (b) lateral adjustment of the bank (e.g., bank erosion/collapse) induced by gravity. The balance between these two processes has been extensively investigated in order to develop analytical solutions of the equilibrium channel profile (e.g., Ikeda & Izumi, 1990, 1991; Izumi et al., 1997; Parker, 1978a, 1978b). However, it was usually neglected that the turbulent flow tends to shape the channel profile slowly (De Vries, 1975), while the width adjustment related to bank erosion/collapse can be much faster (Nagata et al., 2000; Zhao et al., 2020). For instance, Simon (1992) observed that the rate of the width adjustment can reach up to 50 m/year. This is consistent with the short and long sampling frequencies of parameters used in AHG and DHG. This motivated our hypothesis that the different geomorphic relationships represented by AHG and DHG result from the control of lateral adjustment of the bank and flow turbulence, respectively.

2.1.2. Hypothesis 2: Ratio *m/f* and Frictional Resistance

Eliminating Q in $H = cQ^f$ and $U = kQ^m$ (Equation 1), a power law relationship can be deduced between the velocity and the water depth characterized by the ratio m/f (i.e., $U \propto H^{m/f}$). Rhodes (1977, 1987) and Ferguson (1986) used this ratio seeking to decipher the scatter in the *b-f-m* ternary diagram, but only a few values were investigated (e.g., $m/f = 1/2$, $m/f = 2/3$, and $m/f = 1$). The large data set available enable us to notice a continuous change of *b-f-m* exponents with m/f (Figure 2). The AHG data approximately distribute within the interval $0.2 < m/f < 2.2$ and the DHG data mostly concentrate in the interval $0 < m/f < 1.1$. Polynomial regression is employed to fit the curvilinear trends of the AHG and DHG exponents (the thin lines in Figure 2). The *R*-squared values (R^2) of the AHG trendlines are 8%, 73%, and 78% for exponents b_s, f_s, and m_s, and are 17%, 49%, and 86% for the DHG counterparts. The relatively high R^2 values for f and m are largely determined by their implicit correlation to m/f. However, these two data sets do show different trends under the same operation, which highlights how their systematic variability with m/f differ.

The frictional resistance can be expressed in a quadratic form, say $\tau = \rho C_D U^2$, where ρ is the density of water and C_D is the drag coefficient. The value of C_D is determined by the bed roughness length Z_0 and the water depth H, and can be evaluated using a power law, say $C_D = \alpha\left(z_0 / H\right)^{2q}$, where α is a constant coefficient. It thus can be inferred that the frictional resistance is characterized by the ratio U/H^q, which coincides with the geomorphic relationship $U \propto H^{m/f}$. This elicits our second hypothesis: the systematic variability of the AHG and DHG exponents physically depends on the frictional resistance characterized by the ratio m/f (denoted as q hereafter). This hypothesis also resonates with the suggestions of several researchers (Ferguson, 1986; Leopold et al., 1964; Richards, 1973) who had attempted to link the hydraulic geometry to the frictional resistance.

2.2. Theoretical Models

An idealized channel cross section is developed to investigate the two hypotheses proposed above. The bed shear stress over the cross section is calculated based on a general momentum and continuity equations in a Cartesian coordinate system (as e.g., Yu & Knight, 1998):

$$\tau - \rho g h\left|S\right| - \phi_1 \frac{\partial}{\partial y}\int_0^h \tau_{yx} dz = 0, \tag{2}$$

$$\int_{-\infty}^{+\infty} hu\,dy = Q, \tag{3}$$

where x and y are the longitudinal and the lateral coordinates (m), τ is the bed shear stress (Pa), ρ is the density of water (kg/m^3), g is the gravity (m^2/s), h is the water depth (m), $|S|$ is the dimensionless hydraulic slope, τ_{yx} is the turbulent shear stress (Pa), and ϕ_1 is a Boolean variables, which allows to include/exclude the turbulence term. The momentum balance described by Equation 2 is valid for wide and shallow channels, where the lateral bed slope is small. Another commonly used version has been derived based on an orthogonal curvilinear coordinate system, in which the channel cross section is divided by normals perpendicular to the bed (e.g., D'Alpaos et al., 2006; Fagherazzi & Furbish, 2001; Lundgren & Jonsson, 1964; Pizzuto, 1990). The Cartesian coordinate system employed in this study facilitates the derivations of the theoretical forms.

The bed shear stress is linked to the velocity and the water depth using a general Manning-Strickler formula (Parker et al., 2007):

$$\frac{u_*}{u} = \frac{\sqrt{g}n}{h^q}, \tag{4}$$

where u is the velocity (m/s), n is Manning's coefficient, and q is corresponding to the ratio m/f. The turbulent diffusion is evaluated using an eddy viscosity closure (Falconer, 1993):

$$\int_0^h \tau_{yx} dz = \rho h \nu_e \frac{\partial u}{\partial y}, \tag{5}$$

Table 1
Values of b-f-m Exponents and a-c-k Coefficients of AHG Data Collated From Previous Research

		b-f-m exponents			*a-c-k* coefficients		
Authors	Sites/sources	*B*	*F*	*m*	*a*	*c*	*k*
Lewis (1969)	Sana Muerto	0.34	0.23	0.40	9.70	0.33	0.31
	Toro Negro	0.14	0.19	0.57	14.70	0.71	0.10
	Bauta	0.16	0.24	0.48	9.60	0.58	0.19
	Toro Negro-Matrullas	0.16	0.38	0.46	7.60	0.32	0.39
	Toro Negro-Capilla del Carmen	0.08	0.38	0.50	33.0	0.18	0.17
	Toro Negro-Pesas	0.04	0.30	0.61	33.40	0.33	0.10
	Manati-Morovis	0.13	0.43	0.51	24.0	0.18	0.16
	Manati-Matacaiia	0.36	0.36	0.34	4.40	0.33	0.54
	Manati-Ciales	0.18	0.52	0.32	31.0	0.11	0.26
	Manati-Manati	0.07	0.30	0.71	31.20	0.62	0.04
	Average values	0.17	0.33	0.49	19.90	0.37	0.23
	Brandywine Creek	0.04	0.41	0.55	54.0	0.23	0.10
	Ephemeral Streams	0.26	0.33	0.32	10.0	0.10	1.0
	Flume Channels	0.33	0.52	0.16	2.02	0.27	1.80
	Southwest and Great Plains Streams	0.26	0.40	0.34	26.0	0.15	0.37
	White River	0.38	0.33	0.27	4.0	0.22	1.10
Stall and Yang (1970)	Dan River at Danville	0.07	0.49	0.45	268.0	0.06	0.06
Harvey (1975)	River Ter at Lowley Farm	0.14	0.41	0.44	4.14	0.36	0.73
	Wallop Brook at Wallop House	0.13	0.27	0.59	4.94	0.37	0.53
		0.09	0.54	0.38	5.27	0.48	0.40
Jowett (1998)	River Nar at the Carr	0.18	0.31	0.43	15.80	0.31	0.24
	New Zealand Rivers						

Table 1
Continued

Authors	Sites/sources	*b-f-m* exponents			*a-c-k* coefficients		
		B	*F*	*m*	*a*	*c*	*k*
Mackey et al. (1998)	Massachusetts	0.15	0.31	0.53	25.80	0.34	0.12
		0.22	0.30	0.46	15.90	0.36	0.18
		0.25	0.22	0.53	6.94	0.67	0.22
		0.05	0.30	0.64	13.70	0.38	0.21
		0.04	0.34	0.63	79.30	0.31	0.04
		0.14	0.28	0.55	11.40	0.39	0.25
		0.07	0.29	0.64	22.50	0.48	0.09
		0.11	0.34	0.57	7.20	0.40	0.32
		0.09	0.43	0.48	20.50	0.27	0.18
		0.04	0.39	0.57	28.40	0.34	0.10
		0.14	0.24	0.61	20.0	0.75	0.07
		0.21	0.38	0.42	14.60	0.21	0.33
		0.15	0.29	0.55	11.40	0.39	0.24
		0.34	0.19	0.46	8.39	0.59	0.20
		0.24	0.30	0.45	14.80	0.30	0.24
		0.20	0.29	0.52	26.70	0.29	0.13
		0.22	0.18	0.61	13.90	0.62	0.12
		0.16	0.30	0.53	9.43	0.42	0.25
		0.08	0.21	0.73	61.0	0.55	0.03
		0.18	0.36	0.46	28.70	0.28	0.13
		0.11	0.39	0.50	30.70	0.20	0.16
		0.10	0.25	0.64	56.90	0.44	0.04
		0.25	0.26	0.52	13.10	0.39	0.18
		0.20	0.31	0.49	16.90	0.30	0.20
Dudley (2004)	West Branch Union River at Amherst	0.16	0.32	0.52	28.70	0.34	0.10
	Garland Brook near Mariaville	0.31	0.41	0.28	5.89	0.31	0.55
	Piscataquis River near Dover-Foxcroft	0.20	0.32	0.48	32.80	0.32	0.10
	Passadumkeag River at Lowell	0.16	0.39	0.45	31.80	0.20	0.16
	Sheepscot River at North Whitefield	0.10	0.28	0.62	35.20	0.50	0.06
	Johnson Brook at South Albion	0.51	0.40	0.09	3.22	0.31	1.0
	Togus Stream at Togus	0.22	0.38	0.40	13.50	0.25	0.30
	Swift River near Roxbury	0.05	0.27	0.68	95.10	0.73	0.01
	Nezinscot River at Turner Center	0.11	0.29	0.60	42.0	0.50	0.05
	Royal River at Yarmouth	0.07	0.27	0.66	90.40	0.65	0.02
Stewardson (2005)	South-east Australia	0.11	0.28	0.52	16.0	0.49	0.29
Doheny and Fisher (2007)	Gwynns Falls at Glyndon	0.33	0.27	0.39	3.16	0.46	0.69
	Gwynns Falls near Delight	0.21	0.39	0.41	7.75	0.32	0.41

Table 1
Continued

Authors	Sites/sources	*b-f-m* exponents			*a-c-k* coefficients		
		B	*F*	*m*	*a*	*c*	*k*
Alexander et al. (2009)	Niobrara River	0.12	0.46	0.42	27.0	0.11	0.34
		0.22	0.31	0.39	21.0	0.22	0.31
		0.05	0.39	0.57	53.0	0.17	0.11
		0.10	0.40	0.51	81.0	0.11	0.11
		0.19	0.46	0.35	24.0	0.10	0.41
		0.27	0.34	0.39	34.0	0.15	0.19
		0.01	0.46	0.53	230.0	0.07	0.07
		0.32	0.34	0.34	53.0	0.08	0.23
		0.14	0.40	0.45	91.0	0.12	0.20
Singh (2014)	Brandywine Creek at Cornong	0.09	0.37	0.54	30.59	0.20	0.16
	Brandywine Creek at Lenape	0.08	0.47	0.45	61.20	0.13	0.12

Note. Alexander et al. (2009), Doheny and Fisher (2007), Dudley (2004), Harvey (1975), Jowett (1998), Lewis (1969), Mackey et al. (1998), Singh (2014), Stall and Yang (1970), and Stewardsons (2005).
AHG, at-a-station hydraulic geometry.

where ν_e is the depth-averaged eddy viscosity coefficient (m^2/s) expressed as $\nu_e = \Lambda h u_*$ (Fischer, 1973), in which Λ is a dimensionless coefficient and $u_* = \sqrt{\tau / \rho}$ is the friction velocity (m/s). The evolution of the channel profile is governed by the mass conservation law:

$$\frac{\partial h}{\partial t} = Q_{ed} + \phi_2 \frac{\partial Q_{bl}}{\partial y}, \tag{6}$$

where t is time (s), Q_{ed} is the volumetric erosion-deposition rate (m/s), Q_{bl} is the volumetric lateral bed-slope sediment flux (m^2/s), and ϕ_2 is a Boolean variable, which is used to include/exclude the bed-slope term. The local erosion/deposition is linearly related to the bed shear stress (Mehta, 1986):

$$Q_{ed} = M\left(\frac{\tau}{\tau_e} - 1\right), \tag{7}$$

where M is a reference erosion/deposition rate (m/s), and τ_e is the threshold shear stress (Pa). The lateral bed-slope sediment flux Q_{bl}, without loss of generality, is determined by the local bed shear stress and the bed slope (Parker, 1984):

$$Q_{bl} = N\left(\frac{\tau}{\tau_b} - 1\right)\frac{\partial h}{\partial y}, \tag{8}$$

where N is a reference sediment flux (m^2/s) and τ_b is the threshold shear stress for the lateral movement of sediments (Pa). This formula was developed to model the downslope bedload sediment flux of sand (e.g., Ikeda, 1989), while Talmon and Wiesemann (2006) extended its application to total load transport. The morphodynamic evolution governed by Equations 2–8 can be simulated numerically (as e.g., Pizzuto, 1990; Wobus et al., 2006; Xu et al., 2019), which helps to determine the convergence of the ideal systems. A detailed description of the numerical approach is provided by Xu et al. (2019) and the code is available through the https://doi.org/10.5281/zenodo.3825909.

Note that Hypothesis one is invoked into the system through the Boolean values ϕ_1 and ϕ_2, while the interplay between the fast and slow processes are not explicitly embodied in the simulations or derivations. The strategy is to simulate the ideal equilibrium profiles fully determined by the short-term and long-term processes, respectively, and then to compare the resultant geomorphic relationships with the AHG and DHG data sets, respectively. Hence, two theoretical models are developed with (a) $\phi_1 = 0$ and $\phi_2 = 1$, namely, only bed-slope sediment transport is considered for the lateral adjustment of the profile (denoted as "BS"

Table 2
Values of b-f-m Exponents and a-c-k Coefficients of DHG Data Collated From Previous Research

Authors	Sites/sources	*b-f-m* exponents			*a-c-k* coefficients		
		b	*f*	*m*	*a*	*C*	*k*
Leopold and Maddock (1953)	Mobile River	0.44	0.29	0.29	8.01	1.05	0.11
	Scioto River	0.37	0.43	0.19	16.58	0.38	0.16
	Tennessee River	0.58	0.39	0.04	7.95	0.31	0.40
	Yellowstone River	0.50	0.32	0.18	8.36	0.27	0.45
	Belle Fourche River	0.53	0.24	0.17	8.67	0.20	0.49
	Kansas River	0.50	0.43	0.06	11.88	0.19	0.46
	Missouri River	0.44	0.52	0.04	12.91	0.10	0.77
Miller (1958)	Pecos River	0.59	0.30	0.11	3.0	0.34	0.99
	Rio Santa Barbara	0.49	0.39	0.12	3.50	0.31	0.93
Fahnestock (1963)	White River	0.38	0.33	0.27	4.72	0.22	0.88
	Southwest and Great Plains	0.50	0.40	0.10	7.25	0.63	0.39
	Brandywine Creek	0.57	0.40	0.03	13.25	0.24	0.35
	Ephemeral streams	0.50	0.28	0.22	9.42	0.09	1.0
	Flume channels	0.50	0.39	0.16	7.61	0.22	0.70
	Flume channels	0.33	0.52	0.16	1.98	0.53	0.97
Mikhailov (1970)	Danube Delta	0.48	0.35	0.17	5.96	0.56	0.30
Emmett (1972)	Yukon River	0.50	0.35	0.15	4.33	0.28	0.84
Bray (1973)	Alberta	0.53	0.33	0.14	4.75	0.27	0.79
Emmett (1975)	Salmon River	0.53	0.42	0.05	3.30	0.20	1.52
Griffiths (1980)	New Zealand	0.48	0.43	0.11	7.90	0.21	0.61
Andrews (1984)	Colorado	0.60	0.41	0.06	2.71	0.32	1.25
Elliott and Cartier (1986)	Colorado	0.36	0.43	0.17	4.48	0.31	0.85
Hey and Thorne (1986)	various sites	0.45	0.35	0.20	3.67	0.33	0.83
Rhoads (1991)	Missouri River Basin	0.50	0.34	0.16	9.54	0.57	0.18
Andrén (1994)	Laitaure Delta	0.39	0.39	0.23	10.0	0.36	0.28
Allen et al. (1994)	American Streams	0.56	0.34	0.10	2.71	0.35	1.07
McCandless and Everett (2002)	Maryland Piedmont	0.52	0.42	0.06	2.84	0.26	1.36
Moody and Troutman (2002)	Clear Creek, Power River & Mississippi River	0.45	0.43	0.12	17.0	0.18	0.33
Sweet and Geratz (2003)	Southeastern Plain and Middle Atlantic Coastal Plain	0.41	0.46	0.06	7.22	0.57	0.30
McCandless and Annapolis (2003)	Coastal Plain	0.47	0.40	0.13	4.59	0.41	0.54
	MD Piedmont	0.52	0.42	0.06	2.84	0.26	1.36
	AP/VR	0.47	0.33	0.20	4.31	0.30	0.78
King (2004)	Idaho	0.48	0.35	0.15	4.33	0.29	0.93
Dudley (2004)	Coastal and central Maine	0.50	0.32	0.18	6.09	0.34	0.48
Xu (2004)	Gravel Meandering Rivers	0.46	0.33	0.21	4.08	0.32	0.77
	Gravel Braided Rivers	0.67	0.31	0.02	4.02	0.15	1.62
	Sand Meandering Rivers	0.57	0.23	0.20	3.13	1.12	0.29
	Sand Braided Rivers	0.46	0.44	0.09	21.38	0.07	0.66
Ellis and Church (2005)	Lower Fraser River	0.60	0.25	0.16	2.60	0.76	0.51
Eaton and Church (2007)	Colorado	0.50	0.36	0.14	4.17	0.26	0.92

Table 2
Continued

Authors	Sites/sources	*b-f-m* exponents			*a-c-k* coefficients		
		b	*f*	*m*	*a*	*C*	*k*
Rachol and Boley-Morse (2009)	Southern Lower Michigan Ecoregion	0.46	0.28	0.25	6.20	0.36	0.45
	Southern Michigan Rivers	0.40	0.29	0.27	7.63	0.38	0.41
Magirl and Olsen (2009)	Washington	0.45	0.37	0.18	7.35	0.26	0.52
Mulvihill and Baldigo (2012)	New York	0.43	0.39	0.19	5.67	0.28	0.62
		0.43	0.31	0.26	5.04	0.39	0.51
		0.59	0.40	0.01	2.57	0.20	1.93
		0.56	0.36	0.09	3.02	0.25	1.30
		0.52	0.44	0.04	3.61	0.22	1.24
		0.50	0.29	0.21	4.42	0.29	0.78
		0.60	0.26	0.14	3.20	0.44	0.71
		0.50	0.36	0.14	4.12	0.27	0.88
Bomhof et al., (2015)	Canada	0.48	0.33	0.18	4.65	0.36	0.62
Pugh and Redman (2019)	Ouachita Mountains	0.49	0.38	0.13	4.40	0.24	0.95

Note. Allen et al. (1994); Andrén (1994); Andrews (1984); Bomhof et al. (2015); Bray (1973); Dudley (2004); Elliott and Cartier (1986); Ellis and Church (2005); Emmett (1972, 1975); Fahnestock (1963); Griffiths (1980); Hey and Thorne (1986); King (2004); Leopold and Maddock (1953); Magirl and Olsen (2009); McCandless and Annapolis (2003); McCandless and Everett (2002); Mikhailov (1970); Miller (1958); Moody and Troutman (2002); Mulvihill and Baldigo (2012); Pugh and Redman (2019); Rachol and Boley-Morse (2009); Rhoads (1991); Sweet and Geratz (2003); Xu (2004).

DHS, downstream hydraulic geometry.

hereafter); and (b) $\phi_1 = 1$ and $\phi_2 = 0$, which emphasizes the adjustment of the channel profile to the flow turbulence (denoted as "FT" hereafter). Note that such either or cases do not exist in natural systems. An additional simulation with $\phi_1 = 1$ and $\phi_2 = 1$ was also performed to demonstrate the functionality of the model. Hypothesis 2 is embedded in the Manning-Strickler friction formula (Equation 4). The value of the exponent q in the friction formula is given by the ratio m/f calculated based on the data sets of *b-f-m* exponents.

3. Results

3.1. Numerical Simulations

The equilibrium profiles resulting from the numerical simulations of BS and FT models are shown in Figure 3. The BS profile is composed of a vertical bank and a curved channel portion (see the blue line in Figure 3a). The bed shear stress peaks at the channel axis and thus the convergence of the lateral sediment flux is compensated (see the red line in Figure 3a). The channel edge is characterized by the threshold bed shear stress for the lateral movement of sediments (i.e., $\tau = \tau_b$). The FT model results in a smoother shape without sharp demarcation between the channel and the bank (see the blue line in Figure 3b). The whole profile is characterized by an evenly distributed bed shear stress equal to the threshold value τ_e (see the red line in Figure 3b). This implies a balance of the hydraulic pressure and the lateral turbulent diffusion throughout the channel profile (Xu et al., 2020). In particular, the bed resistance is fully compensated by the lateral turbulent diffusion at the channel edge, where the hydraulic pressure $\rho g S h$ tends to 0. The simulation with both processes included (i.e., $\phi_1 = 1$ and $\phi_2 = 1$) produces an intermediate equilibrium profile (Figure 3c), similar in shape to previous analytical and numerical approaches (e.g., Ikeda & Izumi, 1990; Jung et al., 2013; Parker, 1978a; Pizzuto, 1990).

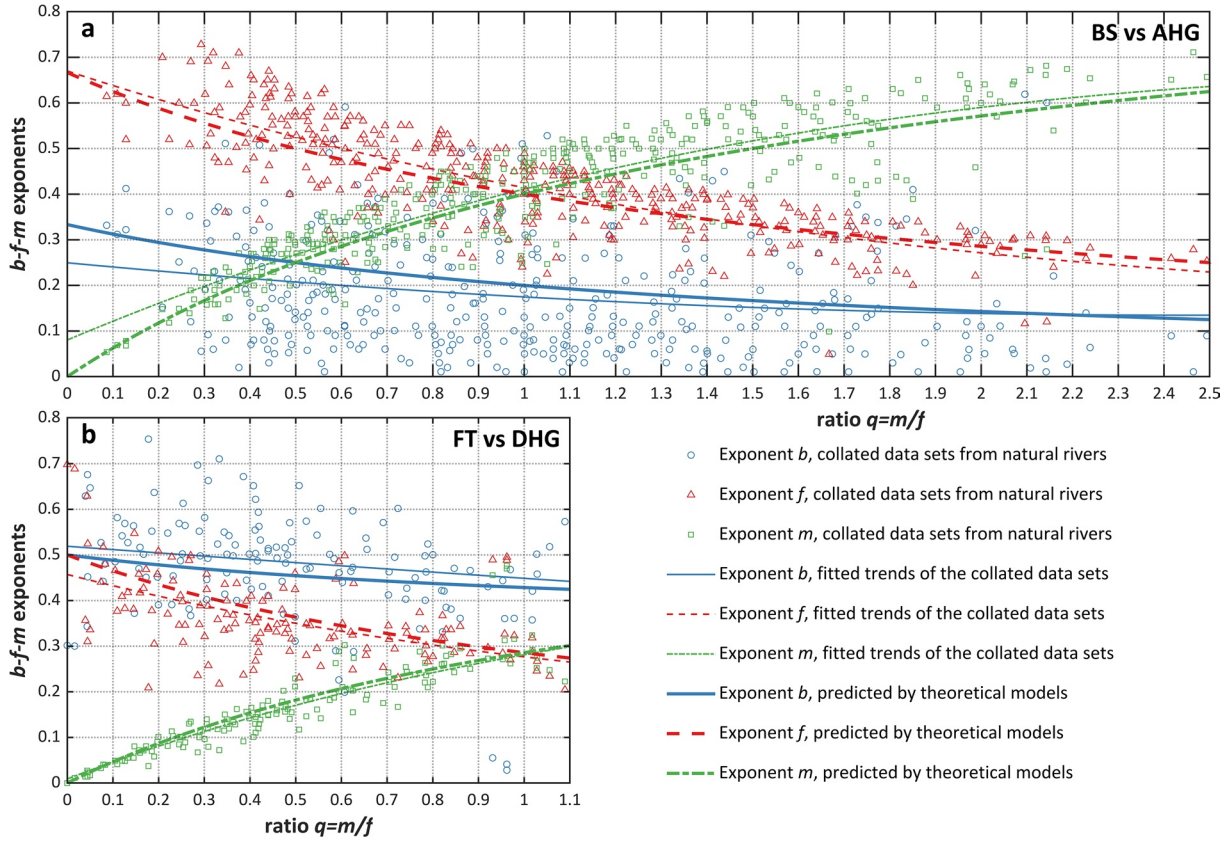

Figure 2. Variability of the collated at-a-station hydraulic geometry (AHG) (points in panel a) and downstream hydraulic geometry (DHG) (points in panel b) exponents with the ratio $q = m/f$, and those predicted by BS (thick lines in panel a) and FT (thick lines in panel b) models, as defined in Section 2.2. The thin lines indicate the trends of the scattered data fitted using polynomial regression. Notice that the AHG data approximately distribute within the interval, $0.2 < q < 2.5$, while the DHG data concentrate in a smaller interval, $0 < q < 1.1$. Hence, panel a is wider than panel b for clarity. The DHG has been redrawn from Xu et al. (2020).

3.2. AHG Parameters (BS Model)

Substituting Equations 2, 7, and 8 into Equation 6 with $\phi_1 = 0$, and imposing $\partial h/\partial t = 0$, the equilibrium profile reached in the BS model is governed by:

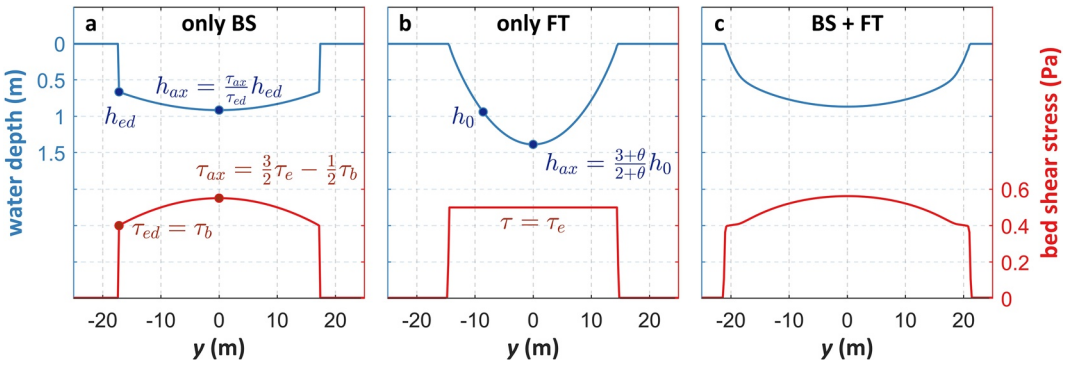

Figure 3. Equilibrium profile reached numerically in (a) Bed-slope (BS) model, (b) Flow turbulence (FT) model, and (c) model with both mechanisms included. The simulations are run with $\tau_e = 0.44$ Pa, $\tau_b = 0.4$ Pa, $\Lambda = 0.8$ (=0 for BS), $M = 5 \times 10^{-8}$ m/s, $N = 10^{-6}$ m^2/s (=0 for FT), $q = 1/6$ and $n = 0.012$ s/m$^{1/3}$. Here the BS profile indicate $h_{ax} \approx 0.91$ m and $h_{ed} \approx 0.67$ m (panel a), and $h_{ax} \approx 1.39$ m for FT (panel b). The width-to-depth ratio of the profiles can cover a broad range of values depending on the parameterization.

$$M\left(\frac{\rho g|S|h}{\tau_e}-1\right)+N\frac{d}{dy}\left[\left(\frac{\rho g|S|h}{\tau_b}-1\right)\frac{dh}{dy}\right]=0, \tag{9}$$

and the solution gives a parabolic profile (Figure 3a):

$$h(y)=-\frac{M\tau_b}{6N\tau_e}y^2+\frac{3\tau_e-\tau_b}{2\rho g|S|}. \tag{10}$$

Based on the criticality at the channel edge (i.e., $h=\tau_b/\rho g|S|$ at $y=B/2$), as confirmed in the numerical simulation (see red line Figure 3a), the width of the profile takes the form:

$$B=6\sqrt{\frac{N\tau_e(\tau_e-\tau_b)}{M\tau_b\rho g}}\frac{1}{|S|^{1/2}}. \tag{11}$$

Then the cross-sectional area and the discharge can be derived by integrations, $A=2\int_0^{B/2}hdy$ and $Q=2\int_0^{B/2}hudy$, giving:

$$A=6\sqrt{\frac{N\tau_e^3(\tau_e-\tau_b)}{M\tau_b\rho^3g^3}}\frac{1}{|S|^{3/2}}, \tag{12}$$

$$Q=\frac{3(3\tau_e-\tau_b)^{q+(3/2)}}{2^{q+(1/2)}ng^{q+2}\rho^{q+2}}\sqrt{\frac{N\tau_e(\tau_e-\tau_b)}{M\tau_b}}\,{}_2F_1\left(\frac{1}{2},-q-\frac{3}{2};\frac{3}{2};\frac{3\tau_e-3\tau_b}{3\tau_e-\tau_b}\right)\frac{1}{|S|^{(3/2)+q}}, \tag{13}$$

where $F_{12}(\alpha,\beta;\gamma;z)$ is a hypergeometric function (Abramowitz & Stegun, 1966), with α, β, γ, and z being constant parameters. Note that all the parameters except for the hydraulic slope $|S|$ are known values in Equations 11–13. Merging these parameters into $\mathcal{B}_s$, $\mathcal{A}_s$, and $\mathcal{Q}_s$ leads to:

$$(B,A,Q)=\left(\frac{\mathcal{B}_s}{|S|^{1/2}},\frac{\mathcal{A}_s}{|S|^{3/2}},\frac{\mathcal{Q}_s}{|S|^{(3/2)+q}}\right), \tag{14}$$

which are all power functions of $|S|$. Equation 14 demonstrates that the BS profile strictly abides by the power law formed geomorphic relationships as presented in Equation 1. Eliminating $|S|$ in Equation 14 further gives the functional forms of *b-f-m* exponents and *a-c-k* coefficients:

$$(b_s,f_s,m_s)=\left(\frac{1}{3+2q},\frac{2}{3+2q},\frac{2q}{3+2q}\right), \tag{15}$$

$$(a_s,c_s,k_s)=\left(\frac{\mathcal{B}_s}{\mathcal{Q}_s^{1/(3+2q)}},\frac{\mathcal{A}_s}{\mathcal{B}_s\mathcal{Q}_s^{2/(3+2q)}},\frac{\mathcal{Q}_s^{3/(3+2q)}}{\mathcal{A}_s}\right). \tag{16}$$

3.3. DHG Parameters (FT Model)

Since $\phi_2=0$ in Equation 6 for the FT model, the equilibrium state is characterized by the threshold shear stress τ_e over the cross section (see the red line in Figure 3b). Substituting the equilibrium condition $\tau=\tau_e$ in Equation 2 with $\phi_1=1$, the governing equation for the equilibrium profile achieved in the FT model is obtained:

$$1-\frac{h}{h_0}-\frac{\Lambda}{\sqrt{g}n}\frac{d}{dy}\left(h^2\frac{dh^q}{dy}\right)=0, \tag{17}$$

where $h_0=\tau_e/\rho g|S|$ is a reference water depth (m). This nonlinear second-order O.D.E. does not admit an explicit solution and implies an infinite number of possible equilibrium profiles. Xu et al. (2019) found that

this system converges to a critical solution characterized by the largest width-to-depth ratio, due to eddy diffusion of momentum. Then an implicit relationship between the bed slope and the water depth can be derived following Xu et al. (2019):

$$\left(\frac{dh}{dy}\right)^2 = \frac{2\sqrt{g}n}{q\Lambda h_0 h^q}\left(\frac{h_0}{2+q} - \frac{h}{3+q}\right), \tag{18}$$

The functional forms of the width B, the cross-sectional area A and the discharge Q can further be derived by integration, as used for the BS model (Section 3.2):

$$B = \frac{(3+q)^{(1+q)/2}}{(2+q)^{(1+q)/2}}\sqrt{\frac{2q\Lambda}{\sqrt{g}n}}\mathbb{B}\left(1+\frac{q}{2},\frac{1}{2}\right)h_0^{(1+q)/2}, \tag{19}$$

$$A = \frac{(3+q)^{(2+q)/2}}{(2+q)^{(3+q)/2}}\sqrt{\frac{2q\Lambda}{\sqrt{g}n}}\mathbb{B}\left(2+\frac{q}{2},\frac{1}{2}\right)h_0^{(2+q)/2}, \tag{20}$$

$$Q = \frac{(3+q)^{(2+3q)/2}}{(2+q)^{3(1+q)/2}}\sqrt{\frac{2q\tau_e\Lambda}{\rho\sqrt{g^3}n^3}}\mathbb{B}\left(2+\frac{3q}{2},\frac{1}{2}\right)h_0^{(2+3q)/2}, \tag{21}$$

where $\mathbb{B}(\alpha,\beta)$ is a Beta function, where α and β are constant parameters. This derivation follows the work of Xu et al. (2020), where a steady regime discharge was assumed. Merging the coefficients in Equations 19–21 to $\mathcal{B}_d$, $\mathcal{A}_d$, and $\mathcal{Q}_d$, the geomorphic relationships can be expressed as:

$$\left(B,A,Q\right) = \left(\mathcal{B}_d h_0^{(1+q)/2}, \mathcal{A}_d h_0^{(2+q)/2}, \mathcal{Q}_d h_0^{(2+q)/2}\right). \tag{22}$$

Similarly, eliminating h_0 in Equation 22, the geomorphic scales predicted by the FT model also inherently satisfy power law relationships, but with different functional forms of *b-f-m* exponents and *a-c-k* coefficients:

$$\left(b_d, f_d, m_d\right) = \left(\frac{2+q}{4+3q}, \frac{2}{4+3q}, \frac{2q}{4+3q}\right), \tag{23}$$

$$\left(a_d, c_d, k_d\right) = \left(\frac{\mathcal{B}_d}{\mathcal{Q}_d^{(2+q)/(4+3q)}}, \frac{\mathcal{A}_d}{\mathcal{B}_d\mathcal{Q}_d^{2/(4+3q)}}, \frac{\mathcal{Q}_{FT}^{(4+q)/(4+3q)}}{\mathcal{A}_{\mathrm{FT}}}\right). \tag{24}$$

4. Discussion

4.1. *b-f-m* Exponents and *a-c-K* Coefficients

As shown in Section 3, the BS and FT models lead to explicit functional forms of *b-f-m* exponents and *a-c-k* coefficients for AHG (Equations 15 and 16) and DHG (Equations 23 and 24). The next step is to compare the theoretical expressions to parameters extracted from field measurements, including more than 550 sets of *b-f-m* exponents (Park, 1977; Rhodes, 1977, 1987) and up to 120 sets of complete power law relationships giving both *b-f-m* exponents and *a-c-k* coefficients (see Tables 1 and 2). The behavior of the hybrid model (i.e., $\phi_1 = 1$ and $\phi_2 = 1$) depends on the relative influence of the turbulence and the bed-slope term in the FT and BS models respectively. This aspect is illustrated in the supporting information.

Both BS and FT models indicate that *b-f-m* exponents are determined by the ratio $q = m/f$. The BS model (Equation 15) indicates that b and f decrease, and m increases with the ratio m/f (thick lines in Figure 2a), which agrees well with the trends indicated in the data set of AHG exponents (thin regression lines in Figure 2a). In particular, the BS model predicts that $b_s = 0.5\, f_s$ resulting in the parabolic equilibrium profile. Similar relationships have also been reported. For instance, Lewis (1969), Mackey et al. (1998), and Morel

et al. (2019) proposed that $b_s \approx 0.55 f_s$, $b_s \approx 0.533 f_s$, and $b_s \approx 0.467 f_s$ based on averaged AHG exponents measured from different study sites. The *b-f-m* exponents suggested by the FT model (Equation 22) are compared with the data set of DHG exponents (Figure 2b). The theoretical lines (thick lines in Figure 2b) also shows a striking consistency with the regression lines (thin lines in Figure 2b), both exhibiting a decrease in b_d, a relatively rapid decrease in f_d, and an increase in m_d as q increases, $b_d \approx f_d$ as q tends to 0, and $b_d > f_d > m_d$ as $0 < q < 1$.

Jung et al. (2013) analyzed the variabilities of the suspended sediment concentration (SSC) for two types of rivers with DHG $b_d < f_d$ and $b_d > f_d$, respectively. They find that exponent for the concentration as a function discharge (*C-Q*) takes on different values for at-a-station and downstream estimates when $b_d > f_d$ but very similar values when $b_d < f_d$. The work of Kim and Paik (2018), clarifies this as a convergence, as the ratio of b/f gets smaller, rather than a switch based on b being greater or less than f. These studies focus on the steady state condition for given hydraulic geometries and infer the stability of the channel based on the presence or otherwise of an along-channel gradient in sediment concentration. In contrast, the work presented here examines the physical basis of morphological equilibrium and the associated hydraulic geometry. The derived theoretical relationships suggest the AHG should exhibit $b_s < f_s$ (see BS model and Equation 15), whereas the DHG should exhibit $b_d > f_d$ (see FT model and Equation 23). The majority of cases documented in Tables 1 and 2 are in agreement, but eight cases in Table 1 and five rivers in Table 2 do not conform. The possible causes for such inconsistency are discussed in Section 4.3.

The derived *a-c-k* coefficients are determined by several parameters in addition to q, including n, Λ, τ_e, τ_b, M, and N (see Equations 11–13 and 19–21), and thus exhibit larger variability compared to the *b-f-m* exponents. This is in line with the large variability in *a-c-k* coefficients observed in natural systems (Gleason & Smith, 2014; Rhoads, 1991; Stewardson, 2005). However, this also implies a difficulty when trying to verify the theoretical expressions of *a-c-k* coefficients, since existing data sets usually do not provide the information needed to determine those parameters. Therefore, we have endeavored to verify the ranges of the derived *a-c-k* coefficients by imposing rational parameters to the functional forms:

1. The ranges of $q = m/f$ are calculated from the collated *b-f-m* exponents (Figure 2), which give $0 < q < 2.5$ for BS and $0 < q < 1.1$ for FT.
2. The Manning's coefficient is taken as $0.004\ \mathrm{s/m^{1/3}} < n < 0.012\ \mathrm{s/m^{1/3}}$.
3. The dimensionless eddy viscosity is taken as $0.1 < \Lambda < 5$ (Shiono & Knight, 1991; Vionnet et al., 2004)
4. The threshold bed shear stress for erosion τ_e can be calculated based on the Shields' Curve (e.g., Soulsby & Whitehouse, 1997). Here a relatively small range is considered, $0.2\ \mathrm{Pa} < \tau_e < 0.5\ \mathrm{Pa}$. The threshold bed shear stress for lateral sediment flux is assumed to be $0.1\ \mathrm{Pa} < \tau_b < \tau_e$
5. The reference erosion/deposition rate $M = \mathrm{O}(10^{-7})$ (as e.g., Lanzoni & D'Alpaos, 2015). The reference lateral sediment flux, N, can be evaluated by van Rijn (2007) and Talmon et al. (1995)

$$N = \frac{1}{18} d_{50}^{0.9} g^{0.4} h^{0.3} \nu^{0.2} \left(s - 1\right)^{0.4}, \tag{25}$$

where d_{50} is the medium sediment grain size (m), ν is the kinematic viscosity of water ($\mathrm{m^2/s}$), and s is the relative density of sediment. Imposing conventional values of the parameters in Equation 25, such as $5 \times 10^{-5} < d_{50} < 5 \times 10^{-4}$, $0.1 < h < 10$, and $\nu = 1.36 \times 10^{-6}$, it can be deduced that $N = O\left(10^{-7} \sim 10^{-5}\right)$. Since N and M are in symmetric positions in the functional forms (see Equations 10–12), we propose $1 < N/M < 50$.

The comparison is conducted in a semilog coefficient-exponent diagram following Gleason and Smith (2014)'s approach (Figure 4). The complete power law data sets are plotted in *a-b*, *c-f* and *k-m* tuples as scattered points, and the predicted ranges are presented as boxes. The boxes enclose most of the corresponding data points, which implies that the theoretical models predict close-to-reality width-to-depth ratio. The shapes of the boxes are different between BS and FT, while their predictions in the ranges of the *a-c-k* coefficients are similar to each other, both indicating that $c \approx k \ll a$. The points outside the boxes are mainly attributed to their *b-f-m* exponents being higher or lower than the predicted ranges, as constrained by Equations 15 and 23. For example, the BS model predicts that $0.125 < b_s < 0.333$ with $0 < q < 2.5$, while some of the data points indicate a value larger than 0.5 or smaller than 0.1 (blue circles in Figure 4a). Note that a larger ranges parameter would result in larger boxes.

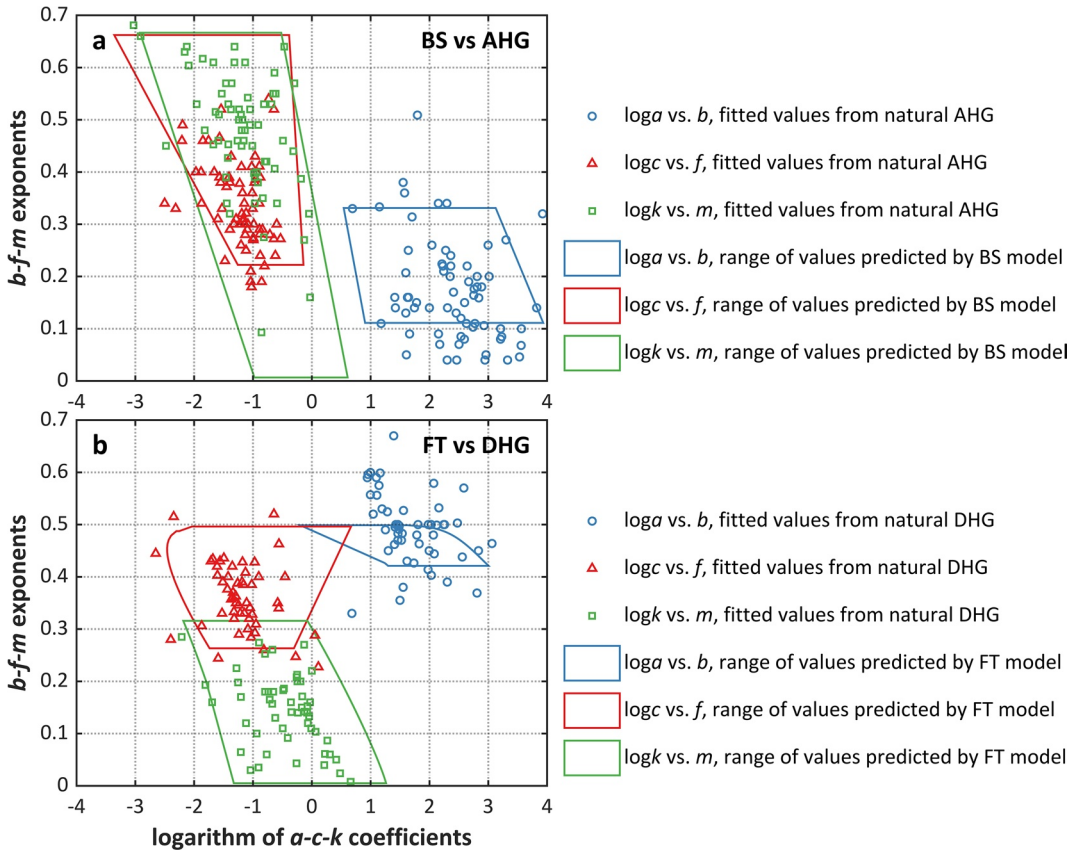

Figure 4. Semilog exponent-coefficient diagram of the data sets (scattered points) and the ranges (boxes) predicted by the Bed-slope (BS) model (Equations 15 and 16) and the Flow turbulence (FT) model (Equations 23 and 24) models. The specific values of the collated *b-f-m* exponents and *a-c-k* coefficients are available in Tables 1 and 2. The ranges of the parameters are given as: $0 < q < 2.5$ for the BS model and $0 < q < 1.1$ for the FT model; Manning's coefficient, 0.004 s/m$^{1/3}$ $< n <$ 0.012 s/m$^{1/3}$; dimensionless eddy viscosity, $0.1 < \Lambda < 5$; threshold bed shear stresses, 0.2 Pa $< \tau_e <$ 0.5 Pa and 0.1 Pa $< \tau_b <$ 0.4 Pa; and the ratio of reference erosion/deposition rate and bed-slope sediment flux, $1 < N/M < 50$. Note that larger ranges of the model parameters can result in bigger boxes.

4.2. Dynamics and Timescales

The predictions of the BS and FT models both exhibit striking consistencies with the large data sets in terms of the systematic variabilities of *b-f-m* exponents as well as the ranges of the *a-c-k* coefficients (Figures 2 and 4). Moreover, a notable improvement is that all these geomorphic relationships are derived based on empirical-theoretical formulations of the underlying processes (e.g., bed resistance, eddy turbulence), rather than a priori determining B, H or U as power functions of Q, or restricting the channel profile to a specific shape. These advantages enable us to provide an explanation on fundamental issues related to the hydraulic geometry.

The ratio m/f expresses how strongly the mean velocity varies with the water depth (i.e., $U \propto H^{m/f}$) and thereby is characterized by the frictional resistance. Hence, the control of m/f on *b-f-m* exponents indicated in both the theoretical models and the data sets (Figure 2) highlights the role of frictional resistance in the systematic variability of both AHG and DHG. This is not surprising, since friction participates in almost all processes that governs the evolution of the channel profile. For instance, in addition to the bottom resistance (Equation 4), friction also affects the lateral momentum exchange resulting from eddy viscosity ($\nu_e = \Lambda h u_*$ in Equation 5), erosion/deposition (τ, in Equation 7), and bed-slope sediment flux (τ, in Equation 8).

The different relationships exhibited by AHG and DHG also provide an example that reflects the duality of morphodynamic systems as change can be driven by different processes operating over different, short

and long, timescales. In this context, Baar et al. (2019) suggested that different calibrations of bed-slope sediment flux are needed to model systems over different spatiotemporal scales. Our theoretical approach suggests that AHG and DHG are governed by lateral bed-slope sediment transport (BS) and FT, respectively (Figures 2 and 4). These two processes can reach an absolute balance with steady boundary conditions as proved in many theoretical and numerical studies (e.g., Parker, 1978b; Pizzuto, 1990, see also Figure 3c). However, natural variability in the discharge tends to continually perturb the system from such an equilibrium configuration. At the same time, BS and FT induce a response to the changing conditions at different speeds and their preferred hydraulic relation can be manifested over short and long timescales.

4.3. Uncertainties in Power Law Relationships

The data sets of AHG or DHG do not exactly conform to the predictions of the theoretical models. The data points of *b-f-m* exponents still show considerable spread around the theoretical lines (Figure 2). Also, the predicted ranges of the *a-c-k* coefficients do not enclose all the data points (Figure 4). These inconsistencies may be related to the simplifications in the theoretical models, including neglecting the spatiotemporal inhomogeneity of bed materials, separating the intertwined processes (i.e., BS and FT), and the assumptions of stationary equilibria (Figure 3), which is rarely achieved in natural systems. On the other hand, the data sets themselves may also contain uncertainties. The relatively large differences between the fitted trends and the theoretical lines of AHG exponents, within the interval $0 < m_s/f_s < 0.2$, may be attributed to the paucity of data points (Figure 2b). As pointed out by Richard (1997), the AHG data are usually measured from relatively stable channel cross sections, where vertical changes in water level are fast compared to changes in width. While this type of channel cross sections improves the accuracy of the flow measurements, it might also lead to an underestimation of the exponent b_s for AHG. Moreover, we are unable to confirm that the collated field data are measured and processed to a uniform standard, or whether the definitions of the width and the depth are consistent, as well as the sampling frequency for the time-varying parameters. These uncertainties should be considered when interpreting the results.

Moving beyond the parameters and into the underlying controversy of the existence of power law relationships. The ability of power law relationships to capture the observations for so many systems around the world has generated many attempts to invoke various forms of "theoretical" explanation. But the data scatter has led to skepticism as to the validity of such relationships and the adequacy of any such theoretical explanation has also been questioned (Bates, 1990; Richards, 1973; Teleki, 1972). In fact, as long as the descriptions of the underlying processes are semiempirical, it is impossible to theoretically demonstrate the power law relationships in a strict sense. The present derivation is no exception. For example, if a logarithmic expression of friction is used (e.g., Colebrook-White), it can be immediately deduced that the geomorphic relationships are not power laws (Julien & Wargadalam, 1995). In fact, the present derivation demonstrates that power laws provide a suitable approximation of AHG and DHG using common expressions of the underlying processes (e.g., frictional resistance and eddy viscosity closure). Notice that we do not a priori restrict the forms of B, H or U as power functions of Q.

4.4. Revisiting AMHG: Can It Be Physically Explained by the BS Model?

Gleason and Smith (2014) plotted a series of fitted AHG parameters along a river using a semilog coefficient-exponent diagram and observed that b_s, f_s, and m_s generally indicate a strong linear decrease with $\log a_s$, $\log c_s$, and $\log k_s$, respectively. They termed this result as AMHG. Gleason and Wang (2015) mathematically explained that such linear trends result from imposing each AHG as a power law. Specifically, suppose we have K sets of geomorphic relationships, $B = a_i Q^{b_i}$ with $i = 1,2,3, \ldots, K$. Taking logarithm on both sides gives:

$$\log B = b_i \log Q + \log a_i , \tag{26}$$

which represents K straight lines in a log-log Q-B plot (Figure 5a). Gleason and Wang (2015) proposed that such a family of AHG yield a perfect AMHG, if all the AHG curves exactly intersect the same point, say

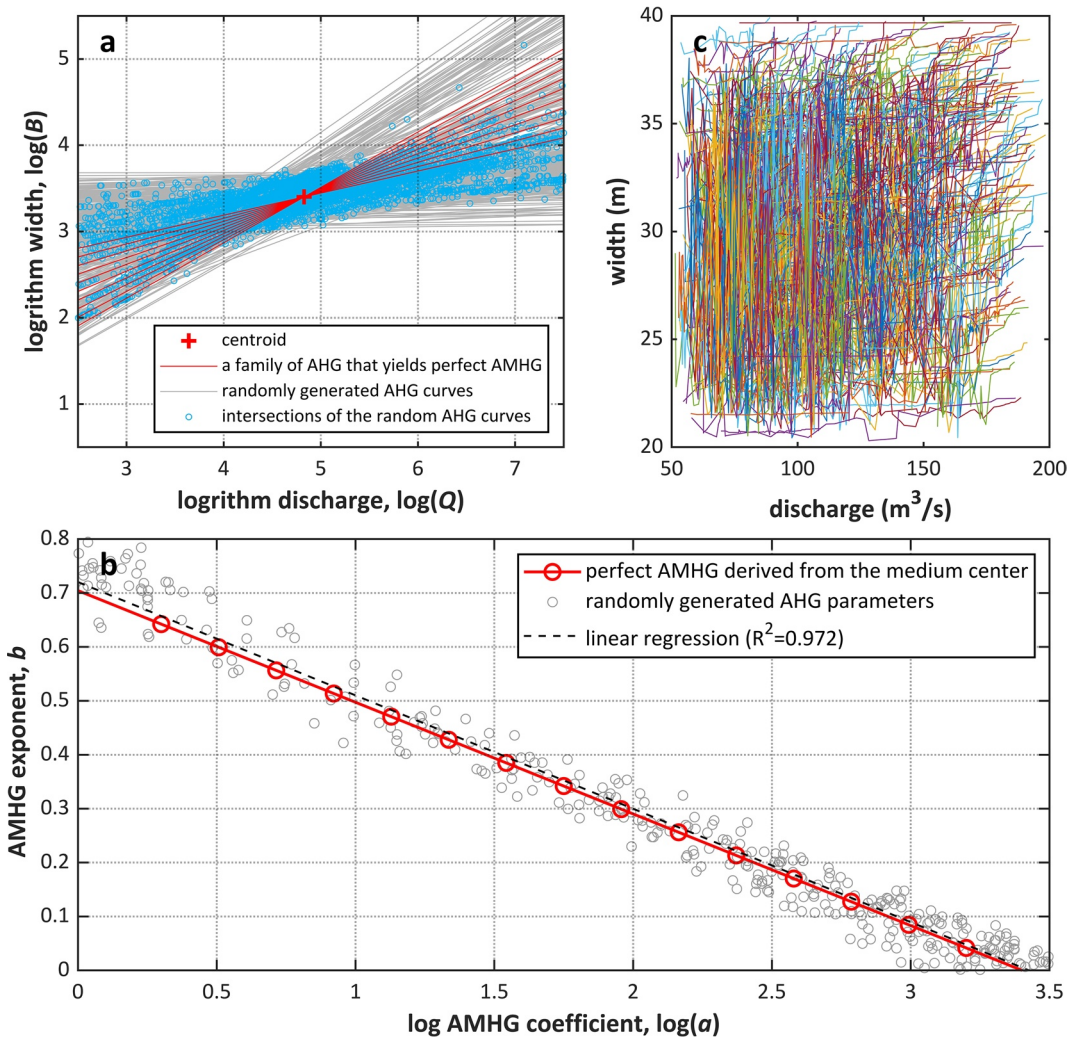

Figure 5. Interpretation of at-many-stations hydraulic geometry (AMHG) based on manipulating the power function. Panel (a) shows a log-log *Q*-*B* plot with a family of at-a-station hydraulic geometry (AHG) (red lines) intersecting exactly at the centroid (red cross), which yields a perfect AMHG property. Panel (b) shows a semilog plot for the variability of *a*-*b* tuples with the red "o-" line indicating the perfect AMHG in Panel (a). Panel (c) indicates 500 randomly generated *Q*-*B* sequences, which lead to AHG curves (gray lines in Panel a) with intersections (blue circles) deviating from the centroid (red cross). The resultant *a*-*b* tuples (gray circles in Panel b) still show a strong linear decrease trend (black dashed line in Panel b) close to the perfect AMHG.

$B = B_0$ and $Q = Q_0$ (e.g., red cross in Figure 5a). In this case, all the a_i-b_i tuples lie on a decreasing line in the semilog coefficient-exponent diagram given by (Figure 5b):

$$b_i = -\frac{1}{\log Q_0}\log a_i + \frac{\log B_0}{\log Q_0}. \tag{27}$$

Gleason and Wang (2015) then suggested that a river is characterized by a strong AMHG, if the intersections of the AHG curves are concentrated around a "centroid." Notice that this explanation essentially is based on the superposition of power law fits to the data and does not exclude cases where the *Q*-*B* data points are poorly represented by a power law. To illustrate this point, we randomly generate 20,000 sets of *Q*-*B* sequences within an interval centered on $\left(Q_0, B_0\right)$ ($50 < Q < 200$ m^3/s and $20 < B < 40$ m). We then pick 500 sequences which, have a regression coefficient, $R^2 < 50\%$, when fitted to a power law. The intersections of the resultant 500 straight fitting lines are scattered in the log-log *Q*-*B* plot (see the gray lines and blue circles

in Figure 5a). However, the corresponding *a*-*b* tuples (gray circles in Figure 5b) still show a strong decrease trends as the "perfect" AMHG suggests (compare the black dashed line and the red line in Figure 5b).

Notice that a large data set (e.g., 500 *Q*-*B* sequences here) is needed to mimic the AMHG trend with random data and the fitted *a*-*b* tuples exhibit a divergent distribution (see gray circles in Figure 5b). On the contrary, the measured *Q*-*B* sequences can result in more concentrated patterns and even a small data set can exhibit a strong AMHG trend (e.g., less than 20 *Q*-*B* sequences as reported by Gleason & Smith, 2014). Gleason and Wang (2015) supposed that this might be attributed to the hydraulic self-similarity of the cross sections along a river, which promotes the concentration of intersections of the AHG curves (i.e., Equation 26). Recently, Brinkerhoff et al. (2019) attempted to confirm the physical existence of AMHG, based on Dingman (2007)'s theoretical model of AHG. Here our concern is more specifically on whether such "self-similarity" can be physically explained by the BS model.

The AMHG data (i.e., a series of AHG parameters along a river) of the six rivers reported by Gleason and Smith (2014) are compared with the BS model (Figure 6). The consistency in the ranges of *a*-*b*, *c*-*f*, and *k*-*m* tuples (Figure 6a) resembles the comparison presented in Section 4.1 (Figure 4a). In terms of the trends, the BS model can produce any curve within the predicted range through calibration. Here, we configure the BS model taking advantage of Equation 15, in which variations of the *b*-*f*-*m* exponents only depend on q. Then each river model is calibrated for hydrodynamic and sedimentary parameters n, M, N, τ_e and τ_b, which are assumed to be constant along the river. The resultant *a*-*b*, *c*-*f*, and *k*-*m* curves approximately show linearly decreasing trends, similar to the distribution of the data points (Figure 6). This demonstrates that the BS model, as configured, is able to reproduce the trends exhibited by AMHG. Notice that here we do not pursue a best fit to the observed data points. The parameters of the model are picked using a simple routine that randomly adjusts parameters (within the ranges derived in Section 4.1) until a minimum is found. In fact, these parameters may vary spatially in natural systems. For example, bed materials are known to vary in a spatially coherent way (Blom et al., 2016). A better elaboration of such coherent variability may further improve the explanatory power of the proposed model.

4.5. Limitations and Suggestions for Future Research

As highlighted in Sections 4.3 and 4.4, uncertainties are implicit in many aspects in the research of hydraulic geometry, including the inhomogeneity of natural systems, the errors in data acquisition, and the usage of semiempirical expressions for underlying processes. These limitations can be misleading when determining the parameters of the hydraulic relations and even the legitimacy of the power laws. Therefore, future research should be devoted to eliminating or reducing such uncertainties. Specifically, we consider that the following aspects are worthy of in-depth investigation:

1. The Cartesian coordinate system is employed in the description of the momentum balance (Equation 2). This approach is valid when the lateral bed slopes of the channel cross sections are generally small. However, for the almost vertical bank formed in the BS profile (e.g., Figure 3a), considering only the vertical profiles of the velocity leads to the underestimation of the bed shear stress on the vertical bank and hence the channel width. A more accurate momentum balance can be achieved using an orthogonal curvilinear coordinate system (e.g., Fagherazzi & Furbish, 2001; Lundgren & Jonsson, 1964; Pizzuto, 1990).
2. We assume a specific friction formula (Equation 4), an eddy viscosity closure assuming an identical turbulent transfer (Equation 5), and a constant threshold shear stress (Equations 7 and 8). Recent works have revealed that a river cross section with heterogeneous bed and bank material deviates significantly from such ideal threshold configuration (Dunne & Jerolmack, 2020; Francalanci et al., 2020). The present derivation in fact is a simplified abstraction useful to emphasize the overall trends of fluvial hydraulic geometry. Future models may improve the predictions with more elaborated description of such heterogeneity.
3. The derived theoretical expressions involve several parameters (q, n, Λ, τ_e, τ_b, M, and N) calibrated using short-term laboratory experiments or field measurements (Section 4.1). New approach is needed to verify the validity of such calibrations over short and long timescales.
4. The analyses of AMHG imply that the parameters used to model the underlying physical processes (e.g., n, τ_e, τ_b, M, and N) may exhibit a spatial coherence as supposed by Gleason and Wang (2015) (see also

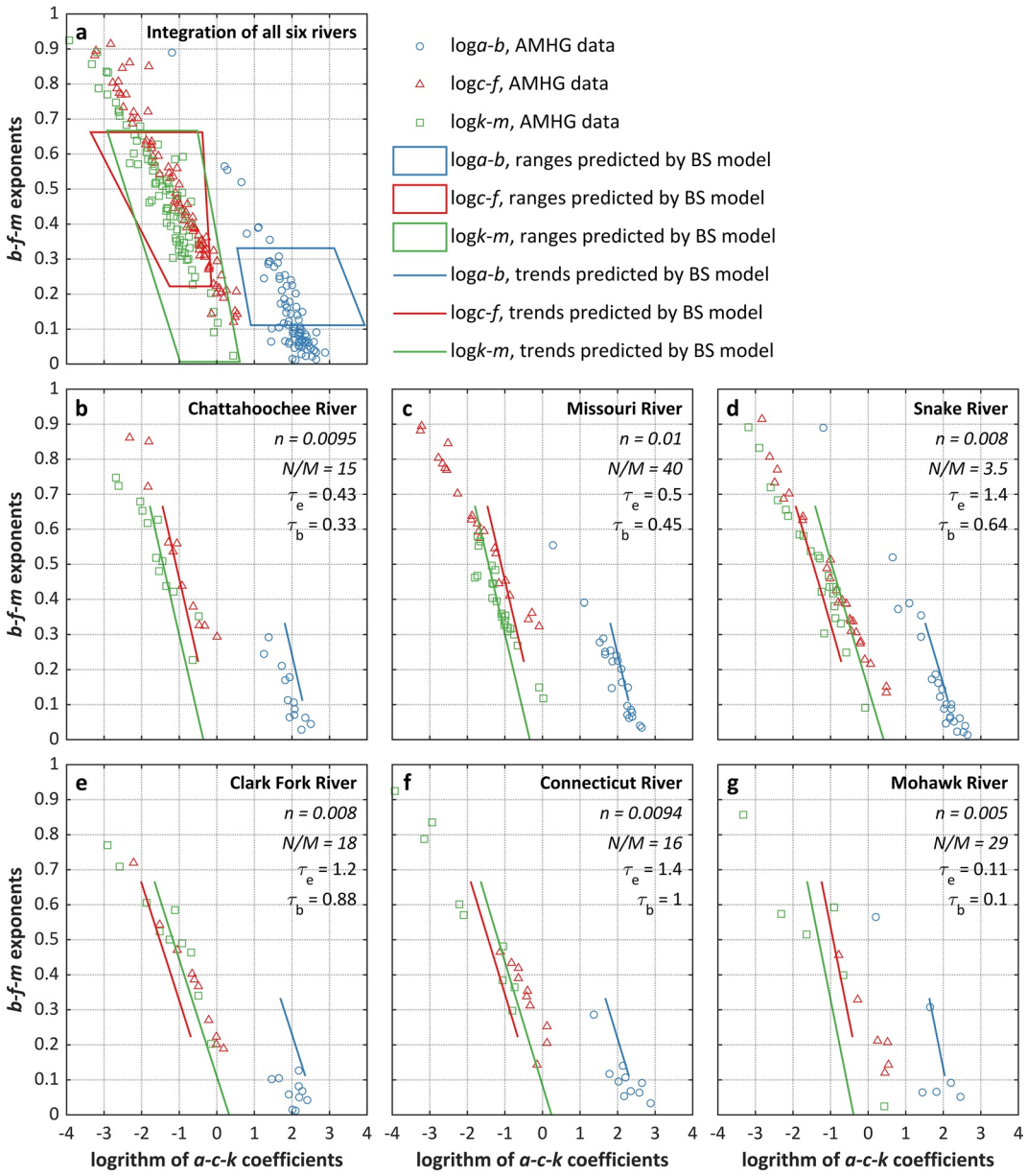

Figure 6. Semilog coefficient-exponent diagram of the at-many-station hydraulic geometry data extracted from Gleason and Smith (2014), and the predictions of bed-slope model. Panel (a) shows the predicted ranges (boxes) and the integrated data of all four rivers (points, as Figure 4a). Panels (b)–(e) compare the predicted trends (lines) to the four rivers (points) separately using different parameters. Note that the length of each line is limited by the predicted range of *b-f-m* exponents (Equation 23).

Section 4.4). This conjecture needs to be confirmed through a careful inspection of the sediment properties along a river, as well as the associated variability of these parameters.

5. Although timescale is highlighted, the specific timescales characterizing BS or FT are not given, nor is the timescale embedded in the derived theoretical expressions. Hence, the variability in the hydraulic relations caused by the interaction of processes operating over different timescales needs further attention.
6. The above suggestions urge us to increase the detail and number of variables measured when testing power law relations. Also, developing standards for the definition and measurement of variables will reduce this source of uncertainty.
7. We stress that the power law formed AHG and DHG are approximations of natural fluvial channels, and that the power law fitting does erase many details relevant to realistic channel geometries. Developing

new theoretical descriptions beyond the power law paradigm is a challenging and valuable direction for future work.

5. Conclusions

Theoretical expressions of AHG and DHG have been derived without any a priori assumptions on the form of the relationship or the cross-sectional shape. The resulting expressions therefore have dimensionally consistent and physically meaningful coefficients. The functional forms of *b-f-m* exponents and *a-c-k* coefficients have been verified using over 550 *b-f-m* exponents and 120 power law hydraulic relations from rivers around the world. In addition, the predicted AHG *a-b*, *c-f* and *k-m* tuples agree well with the at-many-stations hydraulic geometry (AMHG) data exhibiting linearly decreasing trends. The main findings of this study are summarized as follows:

1. The trends of the AHG and DHG exponents are revealed and they both depend on the frictional resistance.
2. The large variability of the *a-c-k* coefficients results from the number of physical and geometric variables present in the theoretical expressions.
3. The different behaviors of AHG and DHG are attributed to the bed-slope sediment transport and the flow turbulence, respectively.
4. Finally, the analysis highlights the uncertainties in the power law formed hydraulic geometry possibly resulting from data acquisition and/or theoretical assumptions.

Data Availability Statement

The code developed in this study are available through the https://doi.org/10.5281/zenodo.3825909. Data sets for this research compiled from the published papers can be downloaded from https://coastalhub.science/data.

Acknowledgments
This study is supported by the National Natural Science Foundation of China (Grant Nos. 42006150, 51739005), Key Program for International S&T Cooperation Projects of China (Grant No. 2016YFE0133700).

References

Abramowitz, M., Stegun, I. A., & Romain, J. E. (1966). *Handbook of mathematical functions: With formulas, graphs, and mathematical tables* (Vol. 55, pp. 120–121). Courier Corporation. https://doi.org/10.1063/1.3047921

Ackers, P. (1964). Experiments on small streams in alluvium. *Journal of the Hydraulics Division*, *90*(4), 1–37. https://doi.org/10.1061/jyceaj.0001060

Alexander, J. S., Zelt, R. B., & Schaepe, N. J. (2009). *Geomorphic segmentation, hydraulic geometry, and hydraulic microhabitats of the Niobrara River, Nebraska—Methods and initial results (Sci. Invest. Rep. 2009–5008)*. Reston, VA: US Geological Survey. https://doi.org/10.3133/sir20095008

Allen, P. M., Arnold, J. C., & Byars, B. W. (1994). Downstream channel geometry for use in planning-level models[1]. *JAWRA Journal of the American Water Resources Association*, *30*(4), 663–671. https://doi.org/10.1111/j.1752-1688.1994.tb03321.x

Andreadis, K. M., Schumann, G. J.-P., & Pavelsky, T. (2013). A simple global river bankfull width and depth database. *Water Resources Research*, *49*, 7164–7168. https://doi.org/10.1002/wrcr.20440

Andrén, H. (1994). *Development of the Laitaure delta, Swedish Lappland: A study of growth, distributary forms and processes*. Sweden: Uppsala University.

Andrews, E. D. (1984). Bed-material entrainment and hydraulic geometry of gravel-bed rivers in Colorado. *Geological Society of America Bulletin*, *95*(3), 371–378. https://doi.org/10.1130/0016-7606(1984)95<371:BEAHGO>2.0.CO;2

Baar, A. W., Albernaz, M. B., van Dijk, W. M., & Kleinhans, M. G. (2019). Critical dependence of morphodynamic models of fluvial and tidal systems on empirical downslope sediment transport. *Nature Communications*, *10*(1), 1–12. https://doi.org/10.1038/s41467-019-12753-x

Barber, C. A., & Gleason, C. J. (2018). Verifying the prevalence, properties, and congruent hydraulics of at-many-stations hydraulic geometry (AMHG) for rivers in the continental United States. *Journal of Hydrology*, *556*, 625–633. https://doi.org/10.1016/j.jhydrol.2017.11.038

Bates, B. C. (1990). A statistical log piecewise linear model of at-a-station hydraulic geometry. *Water Resources Research*, *26*(1), 109–118. https://doi.org/10.1029/WR026i001p00109

Blom, A., Viparelli, E., & Chavarrías, V. (2016). The graded alluvial river: Profile concavity and downstream fining. *Geophysical Research Letters*, *43*, 6285–6293. https://doi.org/10.1002/2016GL068898

Bomhof, J., Rennie, C. D., & Jenkinson, R. W. (2015). Use of local soil and vegetation classifications to improve regional downstream hydraulic geometry relations. *Journal of Hydraulic Engineering*, *141*(5), 4014090. https://doi.org/10.1061/(ASCE)HY.1943-7900.0000978

Bray, D. I. (1973). Regime relations for Alberta gravel-bed rivers. In *Proceeding of hydrology symposium of fluvial processes and sedimentation* (pp. 440–452). University of Alberta.

Brinkerhoff, C. B., Gleason, C. J., & Ostendorf, D. W. (2019). Reconciling at-a-station and at-many-stations hydraulic geometry through river-wide geomorphology. *Geophysical Research Letters*, *46*, 9637–9647. https://doi.org/10.1029/2019GL084529

Cao, S., & Knight, D. W. (1996). Regime theory of alluvial channels based upon the concepts of stream power and probability. *Proceedings of the Institution of Civil Engineers—Water, Maritime and Energy*, *118*(3), 160–167. https://doi.org/10.1680/iwtme.1996.28683

Clifford, N. J. (1996). Classics in physical geography revisited: Leopold, LB and Maddock, TM jr 1953: The hydraulic geometry of stream channels and some physiographic implications. USGS Professional Paper 252. *Progress in Physical Geography*, *20*(1), 81–87. https://doi.org/10.1177/030913339602000105

D'Alpaos, A., Lanzoni, S., Mudd, S. M., & Fagherazzi, S. (2006). Modeling the influence of hydroperiod and vegetation on the cross-sectional formation of tidal channels. *Estuarine, Coastal and Shelf Science*, *69*(3), 311–324. https://doi.org/10.1016/j.ecss.2006.05.002

De Vries, M. (1975). A morphological time-scale for rivers (WL Publ. No. 147). Paper presented at the *XVIth IAHR congress*. Deltares.

Dingman, S. L. (2007). Analytical derivation of at-a-station hydraulic–geometry relations. *Journal of Hydrology*, *334*(1–2), 17–27. https://doi.org/10.1016/j.jhydrol.2006.09.021

Doheny, E. J., & Fisher, G. T. (2007). *Hydraulic geometry characteristics of continuous-record streamflow-gaging stations on four urban watersheds along the main stem of Gwynns falls*. Baltimore, MA. US Geological Survey. https://doi.org/10.3133/sir20065190

Dudley, R. W. (2004). *Hydraulic-geometry relations for rivers in coastal and central Maine*. Denver, CO: US Department of the Interior. https://doi.org/10.3133/sir20045042

Dunne, K. B. J., & Jerolmack, D. J. (2020). What sets river width? *Science Advances*, *6*(41), eabc1505. https://doi.org/10.1126/sciadv.abc1505

Eaton, B. C. (2013). Hydraulic geometry: Empirical investigations and theoretical approaches. *Treatise on Geomorphology*, *9*, 313–329. https://doi.org/10.1016/B978-0-12-374739-6.00243-8

Eaton, B. C., & Church, M. (2007). Predicting downstream hydraulic geometry: A test of rational regime theory. *Journal of Geophysical Research*, *112*, F03025. https://doi.org/10.1029/2006JF000734

Eaton, B. C., Church, M., & Millar, R. G. (2004). Rational regime model of alluvial channel morphology and response. *Earth Surface Processes and Landforms*, *29*(4), 511–529. https://doi.org/10.1002/esp.1062

Elliott, J. G., & Cartier, K. D. (1986). *Hydraulic geometry and streamflow of channels in the Piceance Basin Rio Blanco and Garfield Counties, Colorado* (Vol. 85). Reston, VA: Department of the Interior, US Geological Survey. https://doi.org/10.3133/wri854118

Ellis, E. R., & Church, M. (2005). Hydraulic geometry of secondary channels of lower Fraser River, British Columbia, from acoustic Doppler profiling. *Water Resources Research*, *41*, W08421. https://doi.org/10.1029/2004WR003777

Emmett, W. W. (1972). *The hydraulic geometry of some Alaskan streams south of the Yukon River*. U.S. Department of the Interior, Geological Survey, Water Resources Division. https://doi.org/10.3133/ofr72108

Emmett, W. W. (1975). *The channels and waters of the upper Salmon River area, Idaho*. Washington, DC: United States Goverment Printing Office. https://doi.org/10.3133/pp870A

Fagherazzi, S., & Furbish, D. J. (2001). On the shape and widening of salt marsh creeks. *Journal of Geophysical Research*, *106*(C1), 991–1003. https://doi.org/10.1029/1999JC000115

Fahnestock, R. K. (1963). *Morphology and hydrology of a glacial stream—White river, Mount Rainier* (Vol. 422). Washington, DC: US Government Printing Office. https://doi.org/10.3133/pp422A

Falconer, R. A. (1993). An introduction to nearly horizontal flows. In Abbott & W. A. Price (Ed.), *Coastal estuarial and harbour engineers* (pp. 27–36). London: E and FN Spon LtdE and FN Spon Ltd.

Ferguson, R. I. (1986). Hydraulics and hydraulic geometry. *Progress in Physical Geography*, *10*(1), 1–31. https://doi.org/10.1177/030913338601000101

Finnegan, N. J., Roe, G., Montgomery, D. R., & Hallet, B. (2005). Controls on the channel width of rivers: Implications for modeling fluvial incision of bedrock. *Geology*, *33*(3), 229–232. https://doi.org/10.1130/G21171.1

Fischer, H. B. (1973). Longitudinal dispersion and turbulent mixing in open-channel flow. *Annual Review of Fluid Mechanics*, *5*(1), 59–78. https://doi.org/10.1146/annurev.fl.05.010173.000423

Francalanci, S., Lanzoni, S., Solari, L., & Papanicolaou, A. N. (2020). Equilibrium cross section of river channels with cohesive erodible banks. *Journal of Geophysical Research: Earth Surface*, *125*, e2019JF005286. https://doi.org/10.1029/2019JF005286

Gleason, C. J. (2015). Hydraulic geometry of natural rivers: A review and future directions. *Progress in Physical Geography: Earth and Environment*, *39*(3), 337–360. https://doi.org/10.1177/0309133314567584

Gleason, C. J., & Smith, L. C. (2014). Toward global mapping of river discharge using satellite images and at-many-stations hydraulic geometry. *Proceedings of the National Academy of Sciences of the United States of America*, *111*(13), 4788–4791. https://doi.org/10.1073/pnas.1317606111

Gleason, C. J., & Wang, J. (2015). Theoretical basis for at-many-stations hydraulic geometry. *Geophysical Research Letters*, *42*, 7107–7114. https://doi.org/10.1002/2015GL064935

Griffiths, G. A. (1980). Hydraulic geometry relationships of some New Zealand gravel bed rivers. *Journal of Hydrology*, *19*(2), 106–118.

Harvey, A. M. (1975). Some aspects of the relations between channel characteristics and riffle spacing in meandering streams. *American Journal of Science*, *275*(4), 470–478. https://doi.org/10.2475/ajs.275.4.470

Hey, R. D., & Thorne, C. R. (1986). Stable channels with mobile gravel beds. *Journal of Hydraulic Engineering*, *112*(8), 671–689. https://doi.org/10.1061/(asce)0733-9429(1986)112:8(671)

Huang, H. Q., Nanson, G. C., & Fagan, S. D. (2002). Hydraulic geometry of straight alluvial channels and the principle of least action. *Journal of Hydraulic Research*, *40*(2), 153–160. https://doi.org/10.1080/00221680209499858

Ikeda, S. (1989). Sediment transport and sorting at bends. In I. Syunsuke, & P. Gary (Eds.), *River meandering* (Vol. 12, pp. 103–125). Washington, DC: Wiley Online Library. https://doi.org/10.1029/WM012p0103

Ikeda, S., & Izumi, N. (1990). Width and depth of self-formed straight gravel rivers with bank vegetation. *Water Resources Research*, *26*(10), 2353–2364. https://doi.org/10.1029/WR026i010p02353

Ikeda, S., & Izumi, N. (1991). Stable channel cross sections of straight sand rivers. *Water Resources Research*, *27*(9), 2429–2438. https://doi.org/10.1029/91WR01220

Izumi, N., Ikeda, S., & Parker, G. (1997). Equilibrium cross-sectional shape of straight sand-silt rivers with permeable dikes (pp. 31–41). In *Proceedings-Japan Society of Civil Engineers*. https://doi.org/10.2208/jscej.1997.565_31

Jowett, I. G. (1998). Hydraulic geometry of New Zealand rivers and its use as a preliminary method of habitat assessment. *Regulated Rivers: Research & Management: An International Journal Devoted to River Research and Management*, *14*(5), 451–466. https://doi.org/10.1002/(SICI)1099-1646(1998090)14:5<451::AID-RRR512>3.0.CO;2-1

Julien, P. Y., & Wargadalam, J. (1995). Alluvial channel geometry: Theory and applications. *Journal of Hydraulic Engineering*, *121*(4), 312–325. https://doi.org/10.1061/(asce)0733-9429(1995)121:4(312)

Jung, D., Paik, K., & Kim, J. H. (2013). Relationship between downstream hydraulic geometry and suspended sediment concentration characteristics. *Journal of Hydro-Environment Research*, *7*(4), 243–252. https://doi.org/10.1016/j.jher.2013.03.002

Kellerhals, R. (1967). Stable channels with gravel-paved beds. *Journal of the Waterways and Harbors Division*, *93*(1), 63–84. https://doi.org/10.1061/jwheau.0000482

Kim, D.-H., & Paik, K. (2018). Channel geometry controls downstream lags in sediment rating curves. *Journal of Hydraulic Engineering*, *144*(4), 4018006. https://doi.org/10.1061/(ASCE)HY.1943-7900.0001418

King, J. G., Emmett, W. W., Whiting, P. J., Kenworthy, R. P., & Barry, J. J. (2004). *Sediment transport data and related information for selected coarse-bed streams and rivers in Idaho*. Fort Collins, CO: US Department of Agriculture, Forest Service, Rocky Mountain Research Station. https://doi.org/10.2737/RMRS-GTR-131

Langbein, W. B. (1963). The hydraulic geometry of a shallow estuary. *Hydrological Sciences Journal*, *8*(3), 84–94. https://doi.org/10.1080/02626666309493340

Lanzoni, S., & D'Alpaos, A. (2015). On funneling of tidal channels. *Journal of Geophysical Research: Earth Surface*, *120*, 433–452. https://doi.org/10.1002/2014JF003203

Leopold, L. B., & Maddock, J. T. (1953). *The hydraulic geometry of stream channels and some physiographic implications*. Washington, DC: United States Goverment Printing Office. https://doi.org/10.1016/S0169-555X(96)00028-1

Leopold, L. B., & Miller, J. P. (1956). *Ephemeral streams: Hydraulic factors and their relation to the drainage net* (Vol. 282). Washington, DC: United States Goverment Printing Office. https://doi.org/10.3133/pp282A

Leopold, L. B., Wolman, M. G., & Miller, J. P. (1964). *Fluvial processes in geomorphology*. New York, NY: Dover Publications, Inc. Retrieved from http://pubs.er.usgs.gov/publication/70185663

Lewis, L. A. (1969). Some fluvial geomorphic characteristics of the Manati Basin, Puerto Rico 1. *Annals of the Association of American Geographers*, *59*(2), 280–293. https://doi.org/10.1111/j.1467-8306.1969.tb00671.x

Lundgren, H., & Jonsson, I. G. (1964). Shear and velocity distribution in shallow channels. *Journal of the Hydraulics Division*, *90*(1), 1–21. https://doi.org/10.1061/jyceaj.0000971

Mackey, P. C., Barlow, P. M., & Ries, K. G. (1998). *Relations between discharge and wetted perimeter and other hydraulic-geometry characteristics at selected streamflow-gaging stations in Massachusetts* (Vol. 98). Washington DC: US Department of the Interior, US Geological Survey. https://doi.org/10.3133/wri984094

Magirl, C. S., & Olsen, T. D. (2009). *Navigability potential of Washington rivers and streams determined with hydraulic geometry and a geographic information system*. Washington DC: US Geological Survey. https://doi.org/10.3133/sir20095122

McCandless, T. L., & Annapolis, M. (2003). *Maryland stream survey: Bankfull discharge and channel characteristics of streams in the Coastal Plain hydrologic region*. Annapolis, MD: US Fish & Wildlife Service, Chesapeake Bay Field Office.

McCandless, T. L., & Everett, R. A. (2002). *Maryland stream survey: Bankfull discharge and channel characteristics of streams in the Piedmont hydrologic region*. Annapolis, MD: US Fish & Wildlife Service, Chesapeake Bay Field Office.

Mehta, A. J. (1986). Characterization of cohesive sediment properties and transport processes in estuaries. In *Estuarine cohesive sediment dynamics*. (pp. 290–325). Berlin: Springer. https://doi.org/10.1029/LN014p0290

Mikhailov, V. N. (1970). Hydrologic-morphometric characteristics of delta branches. *Study Report of Hydrology*, *9*, 146–158.

Millar, R. G. (2005). Theoretical regime equations for mobile gravel-bed rivers with stable banks. *Geomorphology*, *64*(3–4), 207–220. https://doi.org/10.1016/j.geomorph.2004.07.001

Miller, J. P. (1958). *High mountain streams: Effects of geology on channel characteristics and bed material*. State Bureau of Mines and Mineral Resources, New Mexico Institute of Mining and Technology.

Moody, J. A., & Troutman, B. M. (2002). Characterization of the spatial variability of channel morphology. *Earth Surface Processes and Landforms. Journal of the British Geomorphological Research Group*, *27*(12), 1251–1266. https://doi.org/10.1002/esp.403

Morel, M., Tamisier, V., Pella, H., Booker, D. J., Navratil, O., Piégay, H., et al. (2019). Revisiting the drivers of at-a-station hydraulic geometry in stream reaches. *Geomorphology*, *328*, 44–56. https://doi.org/10.1016/j.geomorph.2018.12.007

Mulvihill, C. I., & Baldigo, B. P. (2012). Optimizing bankfull discharge and hydraulic geometry relations for streams in New York State. *Journal of the American Water Resources Association*, *48*(3), 449–463. https://doi.org/10.1111/j.1752-1688.2011.00623.x

Nagata, N., Hosoda, T., & Muramoto, Y. (2000). Numerical analysis of river channel processes with bank erosion. *Journal of Hydraulic Engineering*, *126*(4), 243–252. https://doi.org/10.1061/(ASCE)0733-9429(2000)126:4(243)

Park, C. C. (1977). World-wide variations in hydraulic geometry exponents of stream channels: An analysis and some observations. *Journal of Hydrology*, *33*(1–2), 133–146. https://doi.org/10.1016/0022-1694(77)90103-2

Parker, G. (1978a). Self-formed straight rivers with equilibrium banks and mobile bed. Part 1. The sand-silt river. *Journal of Fluid Mechanics*, *89*(1), 109–125. https://doi.org/10.1017/S0022112078002505

Parker, G. (1978b). Self-formed straight rivers with equilibrium banks and mobile bed. Part 2. The gravel river. *Journal of Fluid Mechanics*, *89*(1), 127–146. https://doi.org/10.1017/S0022112078002505

Parker, G. (1984). Discussion of "Lateral Bed Load Transport on Side Slopes" by Syunsuke Ikeda (November, 1982). *Journal of Hydraulic Engineering*, *110*(2), 197–199. https://doi.org/10.1061/(asce)0733-9429(1984)110:2(197)

Parker, G., Wilcock, P. R., Paola, C., Dietrich, W. E., & Pitlick, J. (2007). Physical basis for quasi-universal relations describing bankfull hydraulic geometry of single-thread gravel bed rivers. *Journal of Geophysical Research*, *112*, F04005. https://doi.org/10.1029/2006JF000549

Pizzuto, J. E. (1990). Numerical simulation of gravel river widening. *Water Resources Research*, *26*(9), 1971–1980. https://doi.org/10.1029/WR026i009p01971

Pugh, A. L., & Redman, R. K. (2019). *Regional hydraulic geometry characteristics of stream channels in the Ouachita Mountains of Arkansas*. US Geological Survey. https://doi.org/10.3133/ds1104

Rachol, C. M., & Boley-Morse, K. (2009). *Estimated bankfull discharge for selected Michigan rivers and regional hydraulic geometry curves for estimating bankfull characteristics in southern Michigan rivers*. U.S. Geological Survey. https://doi.org/10.3133/sir20095133

Rhoads, B. L. (1991). A continuously varying parameter model of downstream hydraulic geometry. *Water Resources Research*, *27*(8), 1865–1872. https://doi.org/10.1029/91WR01363

Rhodes, D. D. (1977). The *b-f-m* diagram; graphical representation and interpretation of at-a-station hydraulic geometry. *American Journal of Science*, *277*(1), 73–96. https://doi.org/10.2475/ajs.277.1.73

Rhodes, D. D. (1987). The b-f-m diagram for downstream hydraulic geometry. *Geografiska Annaler—Series A: Physical Geography*, *69*(1), 147–161. https://doi.org/10.2307/521373

Richard, P. I. (1997). Evaluation of optimal channel network and river basin heterogeneity concepts using measured flow and channel properties. *Journal of Hydrology*, *196*(1–4), 119–138. https://doi.org/10.1016/S0022-1694(96)03293-3

Richards, K. S. (1973). Hydraulic geometry and channel roughness: A non-linear system. *American Journal of Science*, *273*(10), 877–896. https://doi.org/10.2475/ajs.273.10.877

Savenije, H. H. G. (2003). The width of a bankfull channel: Lacey's formula explained. *Journal of Hydrology*, *276*(1–4), 176–183. https://doi.org/10.1016/S0022-1694(03)00069-6

Sherwood, J. M., & Huitger, C. A. (2005). *Bankfull characteristics of Ohio streams and their relation to peak streamflows*. US Department of the Interior, US Geological Survey.

Shiono, K., & Knight, D. W. (1991). Turbulent open-channel flows with variable depth across the channel. *Journal of Fluid Mechanics*, *222*(1), 617. https://doi.org/10.1017/s0022112091001246

Simon, A. (1992). Energy, time, and channel evolution in catastrophically disturbed fluvial systems. *Geomorphology*, *5*(3–5), 345–372. https://doi.org/10.1016/0169-555X(92)90013-E

Singh, V. P. (2014). At-a-station hydraulic geometry. In *Entropy theory in hydraulic engineering: An introduction* (pp. 457–514). American Society of Civil Engineers. https://doi.org/10.1061/9780784412725.ch11

Soulsby, R. L., & Whitehouse, R. J. S. (1997). Threshold of sediment motion in coastal environments. In *Pacific Coasts and Ports' 97 Proceedings of the 13th Australasian Coastal and Ocean Engineering Conference and the 6th Australasian Port and Harbour Conference* (Vol. 1, p. 145). Centre for Advanced Engineering, University of Canterbury.

Stall, J. B., & Yang, C. T. (1970). *Hydraulic geometry of 12 selected stream systems of the United States*. U.S. Department of the Interior.

Stevens, M. A. (1989). Width of straight alluvial channels. *Journal of Hydraulic Engineering*, *115*(3), 309–326. https://doi.org/10.1061/(asce)0733-9429(1989)115:3(309)

Stewardson, M. (2005). Hydraulic geometry of stream reaches. *Journal of Hydrology*, *306*(1–4), 97–111. https://doi.org/10.1016/j.jhydrol.2004.09.004

Sweet, W. V., & Geratz, J. W. (2003). Bankfull hydraulic geometry relationships and recurrence intervals for North Carolina's coastal plain. *Journal of the American Water Resources Association*, *39*(4), 861–871. https://doi.org/10.1111/j.1752-1688.2003.tb04411.x

Talmon, A. M., Struiksma, N., & Van Mierlo, M. C. L. M. (1995). Laboratory measurements of the direction of sediment transport on transverse alluvial-bed slopes. *Journal of Hydraulic Research*, *33*(4), 495–517. https://doi.org/10.1080/00221689509498657

Talmon, A. M., & Wiesemann, J.-U. (2006). Influence of grain size on the direction of bed-load transport on transverse sloping beds. In *Proceedings of the 3rd International Conference on Scour and erosion (ICSE-3)* (pp. 632–639). CURNET.

Teleki, P. G. (1972). Areal sorting of bed-load material: The hypothesis of velocity reversal: Discussion. *Geological Society of America Bulletin*, *83*(3), 911–914. https://doi.org/10.1130/0016-7606(1972)83[911:ASOBMT]2.0.CO;2

van Rijn, L. C. (2007). Unified view of sediment transport by currents and waves. I: Initiation of motion, bed roughness, and bed-load transport. *Journal of Hydraulic Engineering*, *133*(6), 649–667. https://doi.org/10.1061/(ASCE)0733-9429(2007)133:6(649)

Vionnet, C. A., Tassi, P. A., & Vide, J. P. M. (2004). Estimates of flow resistance and eddy viscosity coefficients for 2D modelling on vegetated floodplains. *Hydrological Processes*, *18*(15), 2907–2926. https://doi.org/10.1002/hyp.5596

Williams, G. P. (1978). *Hydraulic geometry of river cross-sections: Theory of minimum variance* (Vol. 1029). Washington, DC: US Government Printing Office. https://doi.org/10.3133/pp1029

Wobus, C. W., Tucker, G. E., & Anderson, R. S. (2006). Self-formed bedrock channels. *Geophysical Research Letters*, *33*, L18408. https://doi.org/10.1029/2006GL027182

Wolman, M. G., & Brush, L. M. (1961). *Factors controlling the size and shape of stream channels in coarse noncohesive sands* (pp. 183–210). Washington, DC: US Government Printing Office. https://doi.org/10.3133/pp282G

Xu, F., Coco, G., Tao, J., Zhou, Z., Zhang, C., Lanzoni, S., & D'Alpaos, A. (2019). On the morphodynamic equilibrium of a short tidal channel. *Journal of Geophysical Research: Earth Surface*, *124*, 639–665. https://doi.org/10.1029/2018JF004952

Xu, F., Coco, G., Zhou, Z., Townend, I., Guo, L., & He, Q. (2020). A universal form of power-law relationships for river and stream channels. *Geophysical Research Letters*, *47*, e2020GL090493. https://doi.org/10.1029/2020GL090493

Xu, J. (2004). Comparison of hydraulic geometry between sand-and gravel-bed rivers in relation to channel pattern discrimination. *Earth Surface Processes and Landforms*, *29*(5), 645–657. https://doi.org/10.1002/esp.1059

Yu, G., & Knight, D. W. (1998). Geometry of self-formed straight threshold channels in uniform material. *Proceedings of the Institution of Civil Engineers-Water Maritime and Energy*, *130*(1), 31–41. https://doi.org/10.1680/iwtme.1998.30226

Zhao, K., Gong, Z., Zhang, K., Wang, K., Jin, C., Zhou, Z., et al. (2020). Laboratory experiments of bank collapse: The role of bank height and near-bank water depth. *Journal of Geophysical Research: Earth Surface*, *125*, e2019JF005281. https://doi.org/10.1029/2019JF005281